JMEPEG (2021) 30:8515–8528
https://doi.org/10.1007/s11665-021-06049-9

1059-9495/$19.00

Experimental Investigation of Multiple Laser Shock Peening on Mechanical Properties of Laser Sintering Additively Manufactured Maraging Steel

Tarun Bhardwaj, Mukul Shukla, Arun Kumar Rai, R. Biswal, K. Ranganathan, P. Ganesh, K.S. Bindra, and R. Kaul

Submitted: 23 April 2021 / Revised: 7 June 2021 / Accepted: 18 June 2021 / Published online: 23 July 2021

In this study, the effect of multiple laser shock peening on residual stress, microhardness and tensile properties of direct metal laser sintered Maraging steel 300 is investigated. Multiple laser peening has introduced significant compressive stress in the as-fabricated (−598 MPa) and aged (−653 MPa) samples when compared to the unpeened samples (as-fabricated −270 MPa, aged −310 MPa). Further, it is observed that multiple laser peening led to grain refinement and generation of strain near the surface of laser peened samples. A reduction in crystallite size is observed on increasing the number of laser impacts. The yield strength of laser peened samples is improved by 12.88% and 9.77% in the as-fabricated and aged samples, respectively, in comparison to the unpeened condition. Similarly, the laser peening of as-fabricated and aged samples led to an increase in microhardness by 6.5% and 13.2%, respectively, compared to the unpeened samples.

Keywords direct metal laser sintering, laser shock peening, maraging steel, microhardness, residual stress, tensile properties

1. Introduction

Maraging steel is used as a structural material for various applications due to its ultra-high strength and high toughness. The ultra-high strength is achieved due to precipitation hardening caused by intermetallic compounds during the aging process. To meet the industry demands, development of such materials using laser additive manufacturing (LAM) technology is becoming very popular off late. Recently, the development of Maraging steel using Direct Metal Laser Sintering (DMLS) laser-based Additive Manufacturing is widely pursued as it has the capability to produce near net shape and custom-made 3D metal components. For example, Casalino et al. have optimized the laser processing parameters to develop defect free components of Maraging steel using the Selective Laser Melting (SLM) technique (Ref 1). Suryawanshi, et al. studied the effect of laser process parameters on the mechanical properties of Maraging steel built with SLM (Ref 2). However, the review report of Gu et al. showed that, a difference in thermal history for the deposited subsequent layers results in the generation of tensile residual stresses, leading to premature cracks in the as-fabricated parts (Ref 3). It has been noticed that early crack formation reduces the static and dynamic strength of the physical parts (Ref 4). In particular, the induced tensile residual stresses and porosity formation during LAM fabrication are the main reasons for material failure (Ref 5).

Different techniques such as shot peening, ball burnishing, water jet peening and laser shock peening (LSP) are being used to reduce the tensile residual stresses. Among the above-mentioned techniques, LSP has an advantage over the others due to its capability of introducing larger and deeper compressive residual stresses (CRS) as demonstrated by Ganesh and Rai et al. in ferritic steel (Ref 6, 7). High CRS in the material enhance the static and dynamic mechanical behavior of parts. Lu and Ganesh et al. have demonstrated that when compared to other conventional processes the LSP process has superior capability to improve the surface integrity by inducing high CRS in metallic alloys (Ref 8, 9). In this process, a high intensity ultra-short laser impact is applied on the surface of a pre-coated specimen to generate the shock waves which further propagate into the material and results in deformation. The specimen surface is coated with a sacrificial tape to avoid any thermal exposure which in turn minimizes the development of undesirable tensile residual stresses (TRS) (Ref 10). A schematic representation of the LSP principle is shown in Fig. 1.

To increase the shock waves impact or peak pressure, transparent layer of water is also used as a plasma confining medium (Ref 11). To deform the material plastically and generate high CRS, the peak pressure should exceed the dynamic yield stress of the substrate or Hugoniot elastic limit (HEL). The peak pressure generated by laser shock wave is influenced by absorbed laser energy density (Ref 11) and expressed as follow.

$$P = 0.01\sqrt{[\alpha/(2\alpha+3)](ZI_o)} \quad \text{(Eq 1)}$$

where P (GPa) is the peak pressure, α is the ratio of thermal to internal energy of the plasma (0.3-0.5), Z is the reduced acoustic impedance [$2/Z = 1/(Z_1+Z_2)$] of the confining (Z_1) and

Tarun Bhardwaj, Ajay Kumar Garg Engineering College, Ghaziabad, India; and Motilal Nehru National Institute of Technology Allahabad, Prayagraj, India; **Mukul Shukla**, Motilal Nehru National Institute of Technology Allahabad, Prayagraj, India; and **Arun Kumar Rai, R. Biswal, K. Ranganathan, P. Ganesh, K.S. Bindra,** and **R. Kaul**, Raja Ramanna Center for Advanced Technology, Indore, India. Contact e-mail: bhardwajtarun@akgec.ac.in.

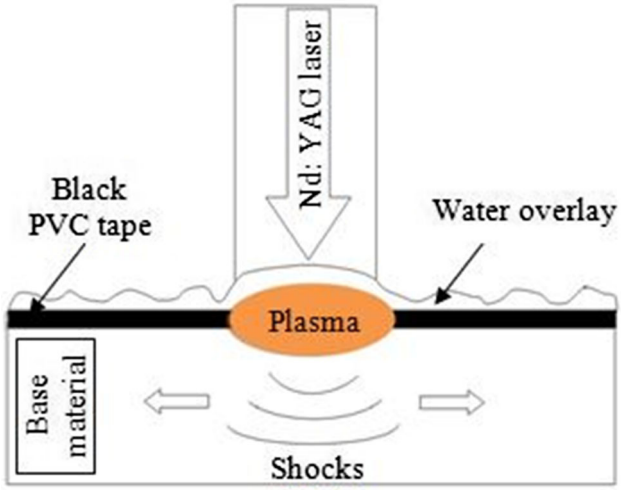

Fig. 1. Schematic representation of the LSP principle

target (Z_2) materials, and I_0 (GW/cm^2) is the absorbed laser power energy density.

Deep CRS below the surface can be generated by providing the laser shock on the surface. Several research studies have been reported on laser shock peening effect on microstructure and mechanical properties of AM materials. For example, Lu et al. (Ref 12) observed the improvement in mechanical properties and refinement in microstructure of AM Ti-6Al-4V using LSP. They reported the formation of large number of mechanical twins in coarse α' martensite after LSP leading to fracture mode transformation from the mixture of ductile and brittle to ductile fracture. Sun et al. (Ref 13) controlled the microstructure and mechanical properties of wire arc additive manufactured 2319 aluminum alloy using LSP. They found higher percentage of low angle boundaries leading to remarkable increase in yield strength by 72% and change in TRS to beneficial CRS. Luo et al. (Ref 14) presented the study on regaining the fatigue strength of LAMed TC17 alloy using LSP. The fatigue strength of LAMed TC17 alloy is reduced from 401 MPa to 365 MPa. However, it is improved to 451 MPa after LSP treatment. Over many years of research, it has been observed that laser peening with multiple laser impacts is more effective than the single laser impact on CRS values and mechanical properties. For example, Petan et al. (Ref 15) reported the effect of increase in pulse density and spot size on the surface integrity of X2NiCoMo18-9-5 Maraging steel. They reported an increase in surface roughness, residual stress and microhardness after LSP. Maximum compressive stress of −1050 MPa and hardness of 770 HV was achieved for a laser spot diameter of 2 mm due to the lower energy attenuation rate and high overlapping ratio. Salimianrizi et al. (Ref 16) studied the effect of laser peening (beam overlap rates and multiple shots) on the residual stress and surface properties of Al 6061-T6. They reported that an increase in overlap ratio (up to 70%) increases the surface roughness due to removal of absorbing layer. Chen et al. (Ref 17) found the change in microstructure and grain size of pure Ni with increase in number of impacts (1, 3 and 5). They reported an increase in microhardness from 97 HV to 206 HV for 5 laser impacts and hardening of layer depth of 370 µm. The strain hardening is attributed to the dislocation motion barrier by formation of new grain boundaries and dislocation multiplication. The accumulated dislocation results in formation of lamellar boundaries and interconnected boundaries.

In our previous study, we reported the effect of laser scan strategy i.e., bidirectional and cross-directional on the mechanical properties of DMLS Maraging steel (Ref 18). We found that cross-directional scan strategy has better mechanical properties than bidirectional scan strategy due to formation of weak textures. Owing to the application of Maraging steel in aerospace and tooling industry, the aim of this research is to improve the service life by surface treatment using LSP.

To the best of our knowledge, no literature has been published on the effect of LSP of DMLS AM Maraging steel mechanical properties. It is also noticed from the above literature that LSP leading to grain refinement and strain hardening for a certain depth, and it increases as the number of laser shocks increase. In the present study, the influence of multiple LSP on as fabricated (F) DMLS Maraging steel is investigated by two adopting two routes: (a) direct LSP and (b) aging sample (F+A) followed by LSP. Decrease in crystallite size, depth-wise microhardness and residual stress and tensile properties before and after LSP are analyzed.

2. Material and Experimental Procedure

Figure 2 shows a block diagram of the experimental procedure adopted in the present study along with the input and output parameters. The block diagram provides at a glance, the various aspects of the experimental methods adopted in the present study. The details of each step are provided in the following sections.

2.1 Fabrication of Maraging Steel Samples

Spherical shape (15-45 µm size) 18Ni-300 powder supplied by EOS GmbH (Germany) is used in this study to fabricate the Maraging steel samples using DMLS process. The chemical composition of Maraging steel 300 is shown in Table 1. The shape and size of the powder are selected to attain maximum packing density parts in DMLS fabricated samples. Samples are fabricated using EOSINT M280 DMLS equipped with Ytterbium fiber laser available at Central Tool Room and Training Center (CTTC), Bhubaneswar, India. The experimental details of DMLS process adopted for printing the Maraging steel samples are provided elsewhere, and in the present study, only important points are given (Ref 18).

The process parameters selected for sample fabrication is based on our previous study (Ref 18) are laser power (285 W), scan speed (960 mm/s), hatch spacing (0.11 mm) and powder layer thickness (40 µm). The sample is fabricated on the mild steel substrate by preheating at 40 °C. Several samples of 15×15×5 mm^3 size are machined using wire electrical discharge machining (Model: EX-7732C express cut) from the DMLS F samples. Tensile specimens are also fabricated as per ASTM E8 to observe the change in tensile property before and after LSP as shown in Fig. 3(a) and (b).

After fabrication, half of the samples are aged at 480°C for 6 h for analysis. Further, all samples (15×15×5 mm^3 size) are polished with SiC sheets ranging from 300 to 2400 grit size followed by cloth polishing for laser peening and further characterization.

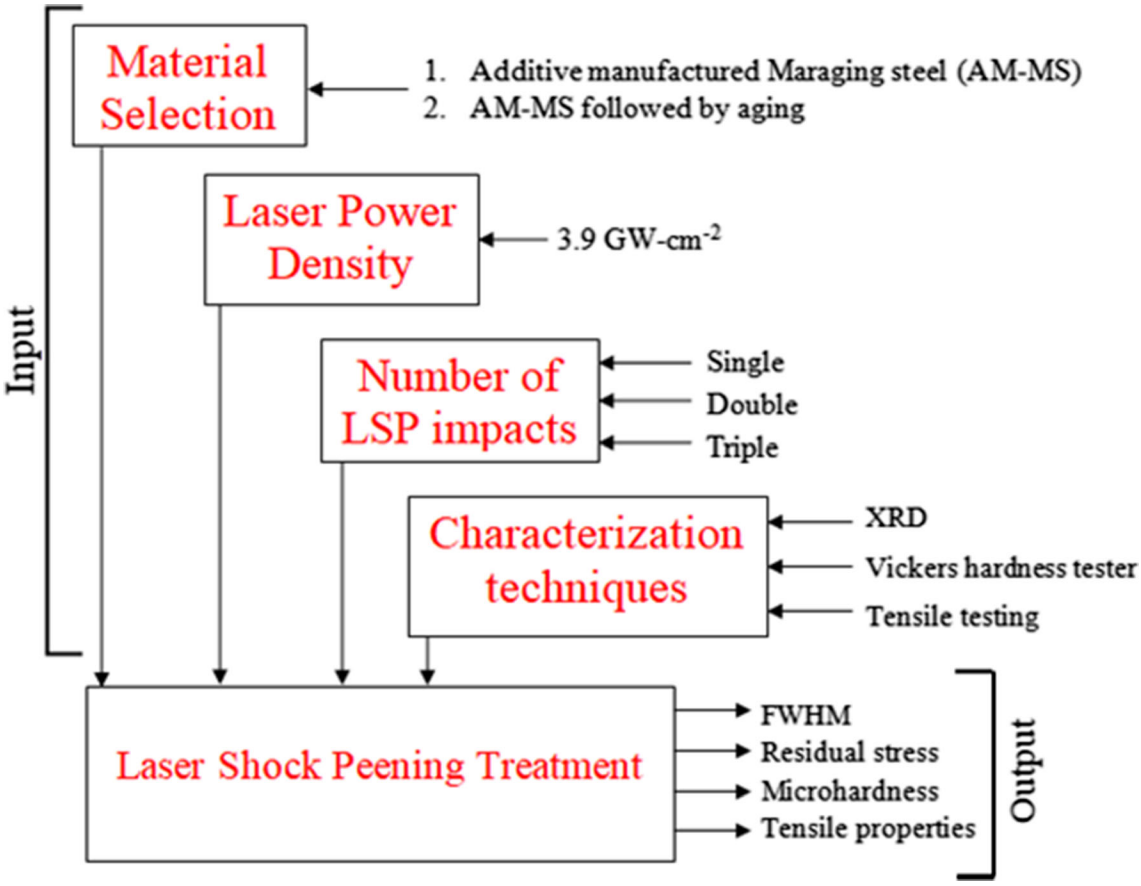

Fig. 2. Block diagram of the experimental setup adopted in the present study

Table 1. Element Composition of Maraging steel 300 powder

Element	Ni	Co	Mo	Ti	Al	Cr, Cu	C	Mn, Si	P, S	Fe
Weight, %	~18	~9	~4.85	~0.7	~0.10	≤ 0.5	≤ 0.03	≤ 0.1	≤ 0.01	Rest

2.2 Laser Shock Peening of DMLS Fabricated Samples

The LSP experiments are performed on the as-fabricated (F) and aged (F+A) Maraging steel samples. The LSP treatment is carried out with an indigenously developed high energy flash lamp pumped electro-optically Q-switched Nd:YAG laser system available at the Laser Technology Division, RRCAT Indore, India. The present laser is an oscillator-amplifier-based system giving a maximum output energy of ~7 J at a repetition rate of 5 Hz with a pulse width <10 ns and beam diameter of ~15 mm ($1/e^2$ points). The experimental parameters used for LSP are selected based on generation of maximum CRS without any material ablation and are shown in Table 2.

The flat top beam laser profile is used for uniform intensity distribution in the peened area. The large spot diameter is kept to attenuate at slower rate of 1/r (r is distance from the laser irradiation point) with planar wave front to achieve deeper compression zone. On the contrary, the small spot diameter generated a spherical wave front and attenuated at the higher rate of $1/r^2$ (Ref 7, 8). To increase the pulse plasma confinement, water overlay of thickness-2-mm is used and to avoid the thermal exposure, black sacrificial PVC tape of 100-μm-thickness is used. The overlap ratio of 71% in scan direction is used to reduce the surface roughness as also mentioned by (Ref 14). Increase in overlap ratio above 71%, leads to tearing of the sacrificing tape layer due to material ablation. Further, multiple peening is done with 1, 2 and 3 impacts at constant laser power density of 3.9 GW cm^{-2}.

2.3 Material Characterization

XRD is performed using an x-ray source of Cu-K_α radiation (λ= 1.54 Angstroms) (RIGAKU model: Smart lab 3 kW diffractometer) with step size of 0.03̊ in the 2θ range of 30̊- 90̊ to obtain the diffraction pattern and analyse full width half maximum (FWHM) distribution for evaluating crystallite size. Further, the residual stress measurements are carried out using Proto Lab iXRD stress measurement system. X-ray diffraction adopting d versus $\sin^2\psi$ method is used to evaluate the residual stresses in the present study. The x-ray source was Cr-K_α radiation (λ= 2.289 Angstroms). The crystallographic plane {211} of α-phase observed at 2θ = 156̊ is monitored at 8 different ψ values to obtain the d versus $\sin^2\psi$ plot for

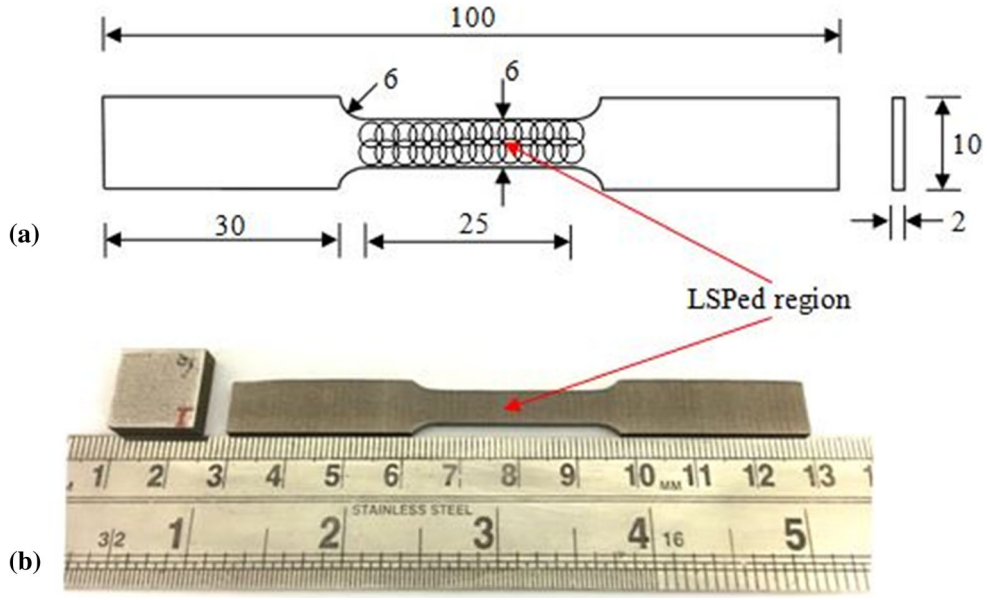

Fig. 3. Tensile specimen (a) dimensions (in mm) and (b) DMLS fabricated specimen

Table 2. Process parameters used for LSP of DMLS Maraging steel

Process parameter	Value
Laser pulse energy	2.5 J
Pulse duration	10 ns
Spot diameter (circular)	3 mm
Laser power density	3.9 GW/cm^2
Repetition rate	2 Hz
Focal length (bi-convex lens)	400 mm
Scan rate	1.75 mm/s
Track to track displacement	1.3 mm
Overlap rate of spots	71%

evaluating the surface residual stress. The elastic modulus of Maraging 300 steel was taken as 206 MPa and Poisson's ratio as 0.25 to calculate the stress values. An average of three measurements is taken to calculate the residual stress of unpeened and peened samples. The x-ray spot size on the sample was kept to 2 mm. The depth-wise residual stress of laser peened samples is measured by progressively removing the surface using chemical etching at an incremental depth of 50 µm. The error associated with residual stress in the present study is found to be of the order of ±25 MPa. The penetration depth of x-ray from Cr source in Maraging steel was of the order of ~4 µm only, and this does not affect much the residual stress data taken across the depth by the chemical etching method. Further, during laser peening the laser spot was kept at 3 mm, and the overlap was maintained at 71% in single peening. To maintain homogeneous peening, multiple laser impacts are applied. Due to this, the variation in residual stress was less than ±15 MPa. Further, the depth-wise microhardness is measured using an Innova tester Nexus 4305. The measurements are conducted on the polished cross-section of the samples at a constant load of 100 g for a dwell time of 15 s. An average of five measurements is taken to calculate the microhardness of unpeened and peened samples. The error associated with microhardness data in the present study was found to be of the order of ± 5 HV. In addition, to obtain the yield stress (YS), ultimate tensile stress (UTS) and elongation (El%), tensile tests are conducted using a universal testing machine of 25 kN load capacity. An average of three samples is taken to evaluate the tensile properties. The LSP is performed on both the sides of the sample gauge length. The error associated with tensile properties in the present study was found be less than 5%

3. Results

3.1 Structural Analysis Using X-ray Diffraction and Crystallite Size Determination

XRD analysis of laser shock peened samples has been carried out to identify the formation of any new phase and microstructural refinement as a result of multiple laser shocks in both the F and F+A samples with respect to the unpeened ones. The XRD spectra of laser peened and unpeened samples with F and F+A condition are presented in Fig. 4 and 5, respectively. Figure 4 and 5 reveal that no new phase is formed after LSP treatment even with increased number of impacts for both the samples, except γ and α′ phases which have been observed in the unpeened sample in the as-fabricated condition. However, it may be noticed from Fig. 4 and 5 that due to the LSP effect, the intensity of martensite phase (α') increases compared to the unpeened F and F+A samples. This could be attributed to the increase in phase fraction of martensite phase as a result of deformation induced martensitic transformation (γ → α') during LSP (Ref 10). In Maraging steel deformation, induced martensite formation is well reported (Ref 14). Further, the formation of deformation induced martensite phase in austenitic and Ti-based alloys are also reported (Ref 13).

It is worth to mention here that peak broadening is also noticed in both samples as a result of LSP. This is due to introduction of high plastic strain and grain refinement (Ref 7,

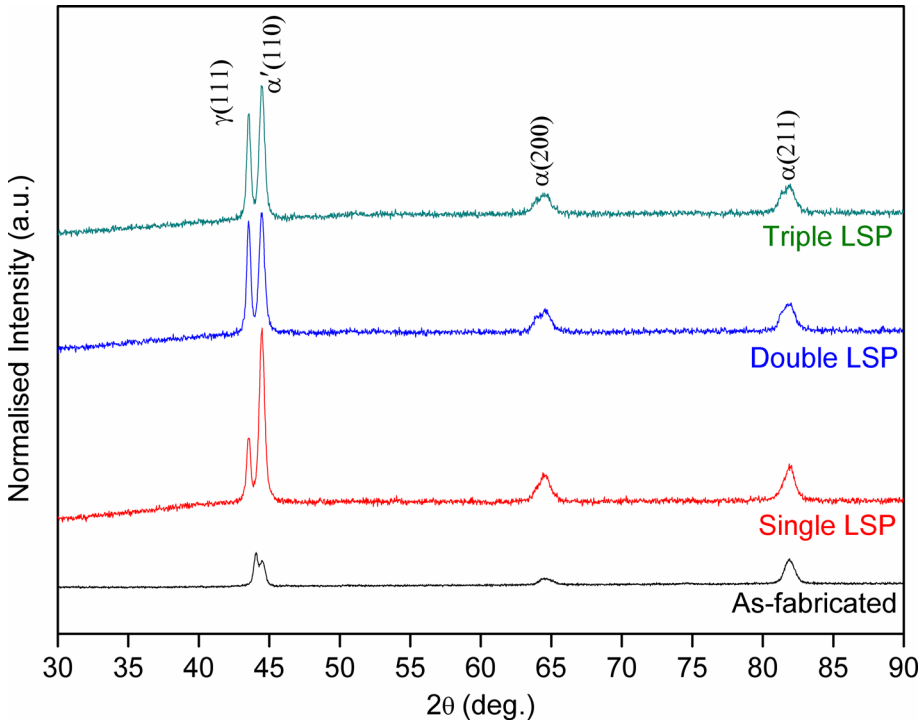

Fig. 4. X-ray diffraction pattern of F and F+LSP samples

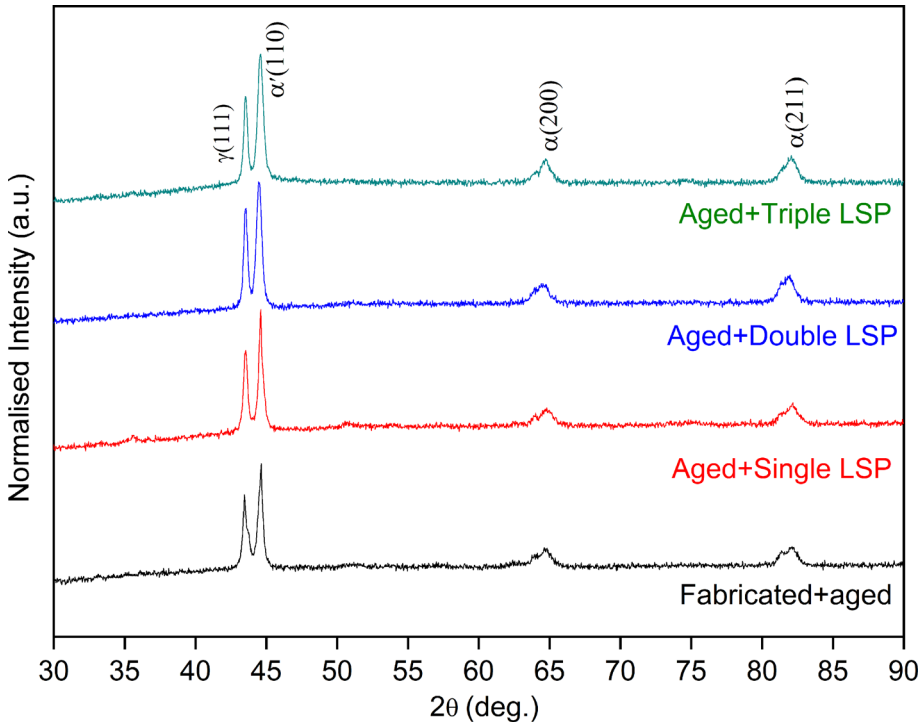

Fig. 5. X-ray diffraction pattern of F+A and F+A+LSP samples

15). This broadening could be arising from grain refinement in sub-micron domain and the presence of high-level of locally existing micro-strain (Ref 7). To quantify the actual broadening effect with respect to the unpeened sample, the full width half maxima (FWHM) has been calculated for individual peaks by line profile analysis, using pseudo-Voigt peak shape function. It is well known that FWHM of a XRD peak is used to characterize different material properties and surface integrity features. The change in FWHM from the normal condition of a material indicates the change in the crystallite size and residual strain in the matrix. The FWHM for different sample conditions (F, F+A, F+LSP and F+A+LSP) is given in Figure 6(a) and (b) for three different diffraction peaks. It is clear that FWHM is increasing with number of laser impacts, which implies

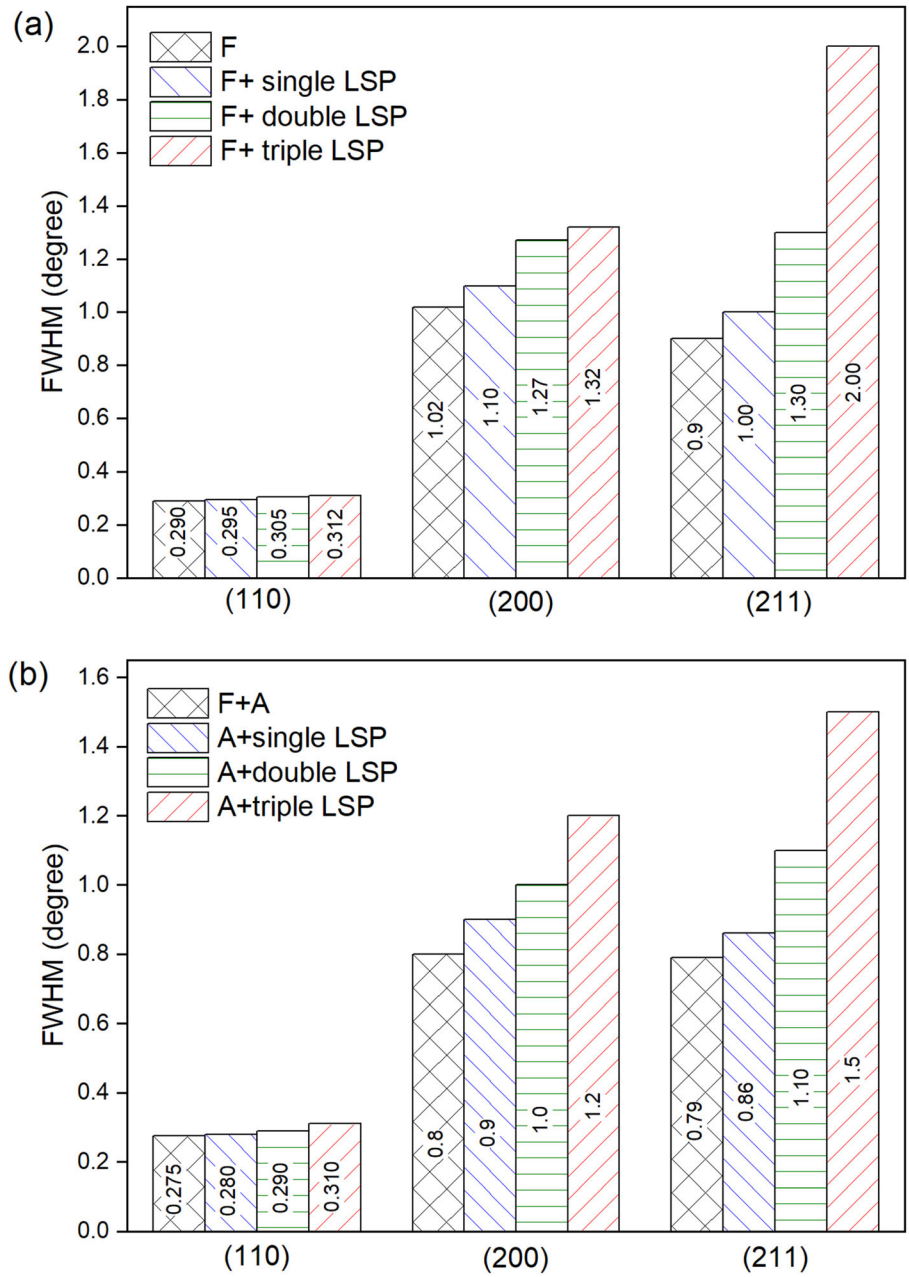

Fig. 6. FWHM for different planes of (a) F and (b) F+A samples before and after multiple LSP

induction of high dislocation density and formation of nano sub-grains (Ref 7, 16). The crystallite size is calculated from XRD data using Williamson-Hall (W-H) approximation approach. The relation of FWHM and crystallite size is co-related using following relation.

$$\beta_{eff} \times \cos\theta = \frac{k \times \lambda}{d} + 4\varepsilon \times \sin\theta \qquad \text{(Eq 2)}$$

where β_{eff} is effective FWHM, θ is the Bragg's angle, k is Scherer's factor (0.9 for spherical grains), λ is the wavelength of x-ray (0.154 nm), d is crystallite size, and ε is strain factor. β_{eff} is calculated using following expression as given in Equation 3:

$$\beta_{eff} = \sqrt{(\beta_{lsp}^2 - \beta_o^2)} \qquad \text{(Eq 3)}$$

where β_{lsp} and β_o are FWHM of LSP and unpeened diffraction peaks.

W-H plots of single, double and triple LSP for F and F+A sample before and after LSP is shown in Fig. 7 and 8, respectively. Line is linearly fitted to obtain the values of intercepts and to calculate the crystallite size using Scherrer's equation. The intercept obtained from W-H plots of single, double and triple LSP are 0.00239, 0.00309 and 0.004, respectively, for F sample and 0.00181, 0.00251 and 0.00337, respectively, for F+A sample. In addition, the slope of W-H plot is also increasing with increasing the number of laser impacts. Therefore, as per Eq (2), it may be confirmed that strain is also getting increased with increasing the LSP impacts.

For single, double and triple LSP, calculated crystallite size is 57 nm, 44 nm and 34 nm, respectively, for F sample and 76

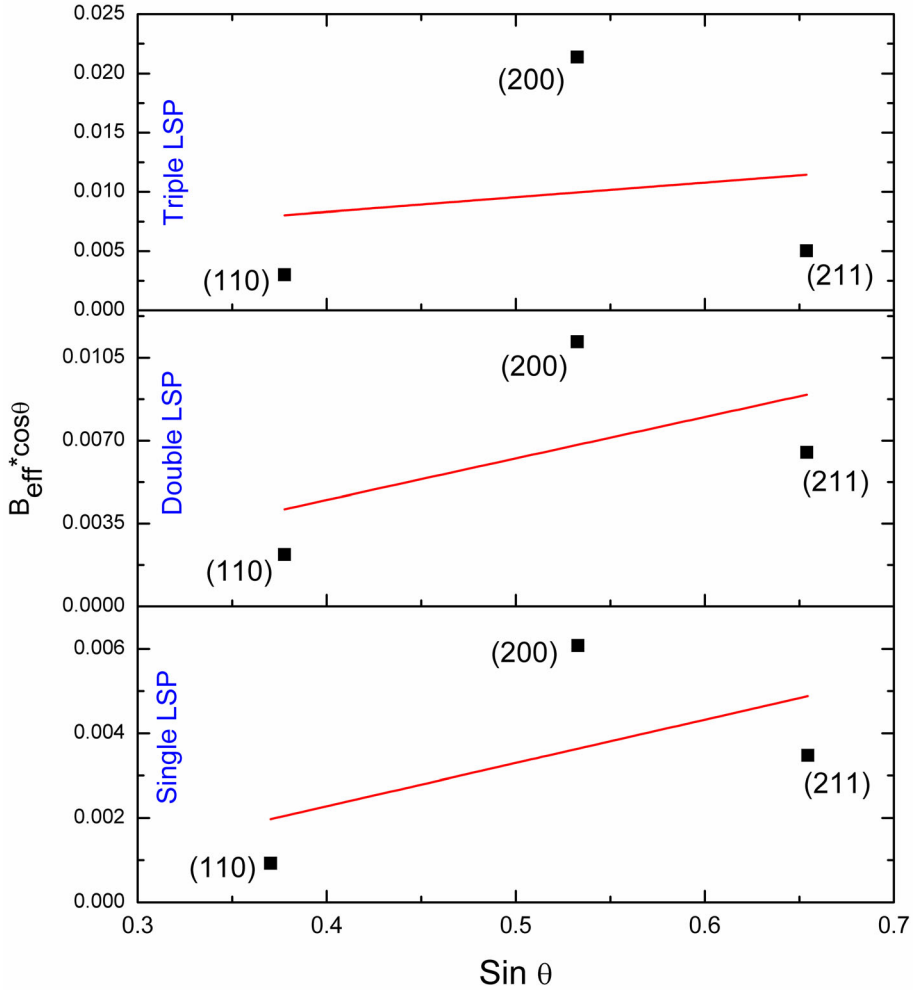

Fig. 7. W-H plots of single, double and triple LSP for F samples along with fitted line

nm, 55 nm and 41 nm, respectively, for F+A sample. Decrease in crystallite size is observed due to high plastic deformation with increase in number of laser shocks leading to an improvement in mechanical properties. The reason behind the reduction in crystal size in laser peened samples will be provided in more detail in the discussion section.

3.2 Effect of Laser Peening on Residual Stress

Residual stress plays a significant role in deciding the service life of the material (Ref 19). It is demonstrated that as the depth of CRS increases from the surface, it leads to increase in the service life. The high CRS is observed in DMLS Maraging steel aged sample due to the martensite crystal lattice expansion during phase transformation from austenite to martensite leads to accumulation of stress (Ref 20). The surface residual stress of DMLS Maraging steel before and after aging for multiple peening is investigated and presented as follows. The surface residual stresses for multiple peening of F and F+A samples are displayed in Fig. 9.

It is observed from Fig. 9 that in the as-fabricated sample post to single peening the compressive residual stress is increased to -517 MPa as compared to the as-fabricated condition (−270 MPa). Further, with increasing the laser impacts, the compressive residual stress is found to be increasing. After triple LSP, the surface residual stress increases from −270 MPa to −598 MPa for the as-fabricated sample. In a similar fashion, for the aged samples, triple peening led to an increase in compressive residual stress to −653 MPa as compared to the unpeened sample (−310 MPa). It may be further inferred that the first LSP impact causes more plastic flow due to low work hardening depth and leads to more plasticity as compared to the double and triple LSP impacts (Ref 21).

It can be shown from Fig. 9 that single LSP increase the surface CRS by 91.48% for F sample and 74.19% for F+A sample in comparison to untreated samples. It is well reported that, increased coverage rate in LSP leads to higher compressive residual surface stress due to generation of high dislocation density, however, it gets saturated after certain number of laser impacts due to annihilation of defect structure and formation of new grains. The high-pressure shock wave generated higher CRS to a deeper depth from the surface, and it increases with the number of impacts (Ref 22). The effect of LSP over depth has also been monitored by measuring the surface residual stress as a function of incremental depth, and the corresponding result is presented in Fig. 10. It can be observed that in the as-fabricated sample the compressive residual stress is only up to a depth of 50 μm, however, after triple peening the compressive residual stress is found to be up to a depth of 675 μm in the as-

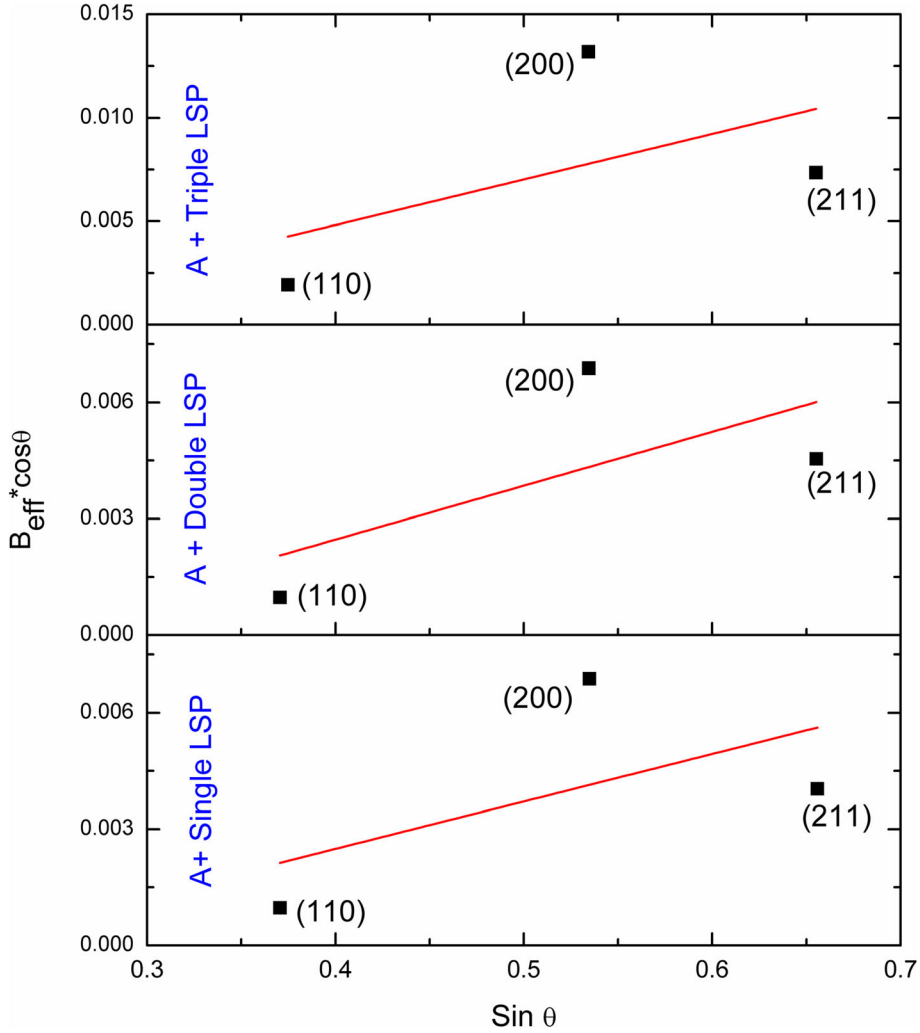

Fig. 8. W-H plots of single, double and triple LSP for F+A samples along with fitted line

fabricated sample and up to a depth of 340 μm in the aged sample.

Owing to low stress attenuation effect, higher depth is observed in the triple LSP F and F+A samples. The low stress attenuation in triple LSP samples is due to generated work hardening layer by the high-pressure shock wave for single and double LSP. The change in residual stress in the F sample from compressive to tensile is observed at 50 μm depth while for the triple LSP F and F+A samples, it is at 675 μm and 340 μm, respectively. Similar kind of increasing nature of CRS with LSP of AM Ti-6Al-4V, 316L and 15-5 PH steel has been observed (Ref 23–25). However, it reaches toward saturation after triple LSP impacts and beyond triple LSP, no significant effect is observed.

3.3 Effect of Laser Peening Parameters on Microhardness

To study the effect of laser shock peening parameters on hardenability of Maraging steel in the present study, the microhardness data are measured as a function of depth from the laser peened surface for both the as-fabricated and aged samples, and the corresponding results are presented in Fig. 11 and 12, respectively. It may be inferred from Fig. 11 that in the case of untreated sample, the hardness data are varying in the range of 395 to 400 HV, however, post to single peening, the hardness data on the surface are increased to 415 HV. Further, with an increase in LSP impacts, the hardness is found to be increasing and for triple peened sample, it has increased to 425 HV. Moreover, across the depth hardness data are found to be gradually reducing and reaches to a base value after a depth of 175 to 250 μm for single and triple LSP impacts, respectively. Similar kind of variation in hardness data of LSP treated Maraging steel with aged condition is also observed, and this may be witnessed in Fig. 12. From Fig. 12, it is clear that the hardness of unpeened samples with aged condition is around 570 HV, and it increased to 620 HV, 638 HV and 640 HV for single, double and triple LSP sample, respectively. Further along the depth again the hardness is found to be decreasing gradually.

The hardened layer depth in case of aged samples is increased from 135 μm for single LSP to 150 μm for double LSP and 220 μm for triple LSP samples. An increase in microhardness is caused due to the decrease in crystallite size and higher dislocation density (Ref 17, 24). However, it reaches to a saturation value after three impacts due to generation of dislocation stacks which impeded the dislocation movement further.

Microhardness of the F+A sample is measured and found to be higher in comparison to the F sample due to the formation of

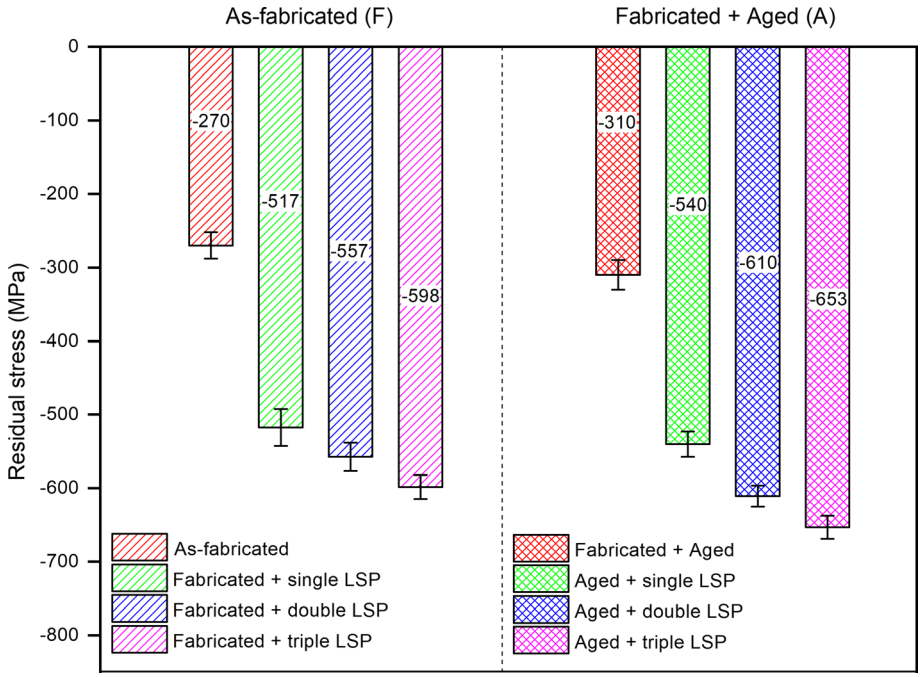

Fig. 9. Surface residual stresses of F and A samples after multiple LSP

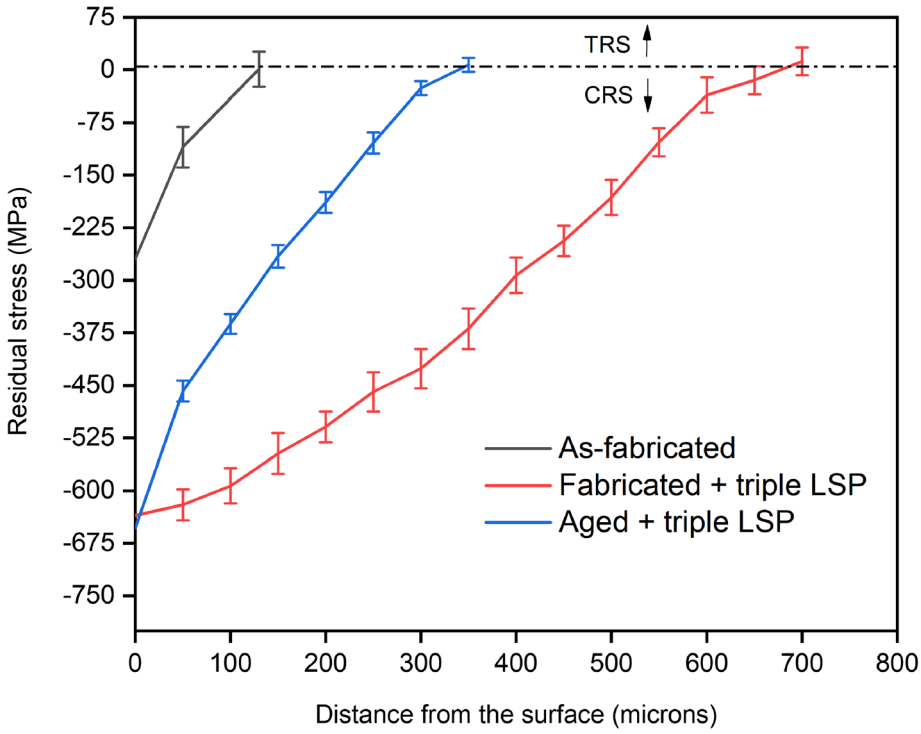

Fig. 10. Depth-wise distribution of residual stress of F and triple LSP F and F+A samples

intermetallic precipitates, leading to impede the dislocations. The microhardness on the surface of the F+A sample is 565 HV and for the F+A sample, an increase in microhardness by 13.2% for triple LSP samples is obtained.

3.4 Effect of Laser Peening on Tensile Properties

The effect of triple LSP on tensile properties is studied for the as-fabricated and the aged Maraging samples at room temperature. The engineering stress-strain curve of F and F+A samples before and after triple LSP is displayed in Fig. 13(a) and (b).

It is found from figures that no significant effect is observed in the linear region for both the conditions. It suggests that no change is occurring in the Young's modulus as also observed by others (Ref 26). However, the yield strength (YS) is found to increase for both the sample types. The YS increases from 753

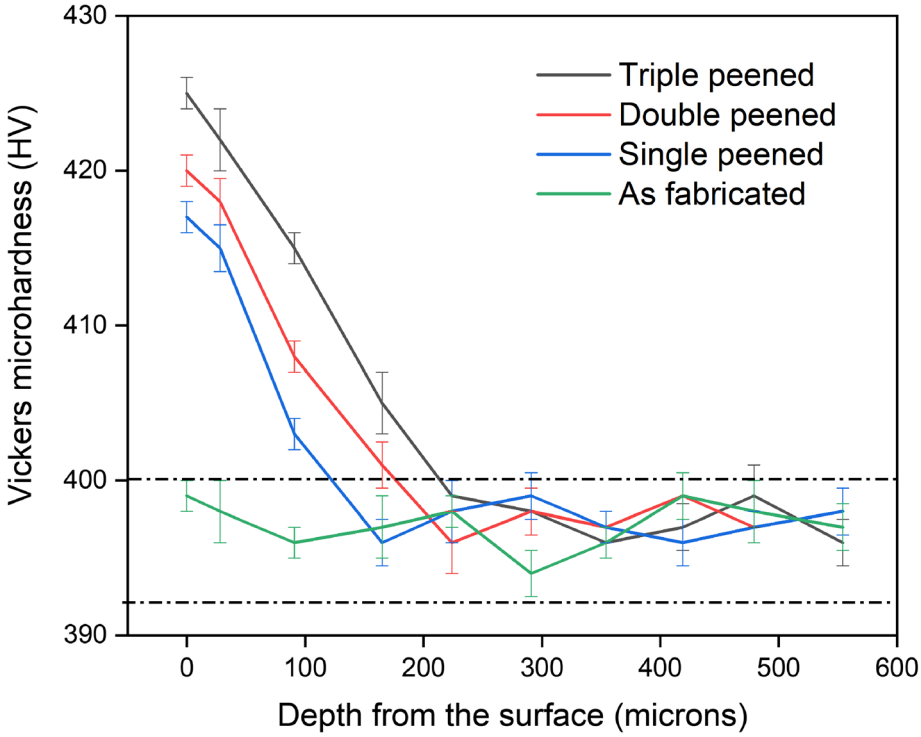

Fig. 11. In-depth microhardness distribution of F and F+LSP samples

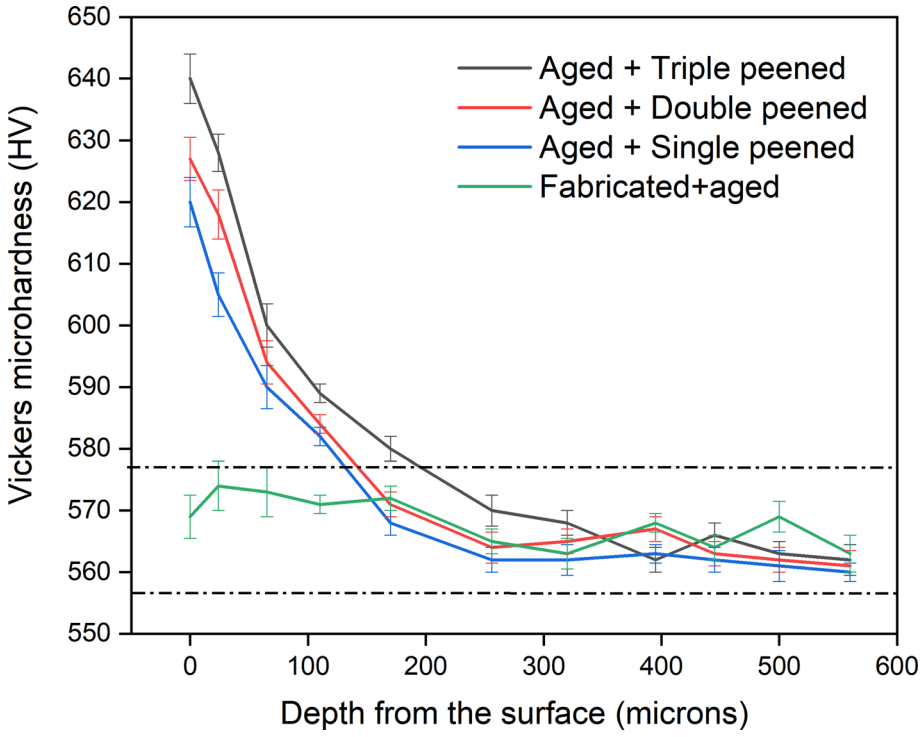

Fig. 12. In-depth microhardness distribution of A and F+A+LSP samples

± 10 to 850 ± 14 MPa and 1740 ± 42 to 1910 ± 43 MPa for the F and A samples, respectively. This increase in YS is attributed to the strain hardening caused by interaction of moving dislocation and diffusive solute atoms by multiple LSP impacts (Ref 27). In addition, decrease in crystallite size due to applied CRS on both sides of tensile samples for both conditions is also a factor of increase in YS. Small change in UTS is found due to peening effect on both F and F+A samples. The UTS changes from 1082 ± 62 to 1120 ± 48 MPa and 1940 ± 24 to 2040 ± 34 MPa for F and F+A samples, respectively, post to triple LSP treatment. Moreover, the magnitude of elongation is found to decrease from 17.5% for F sample to

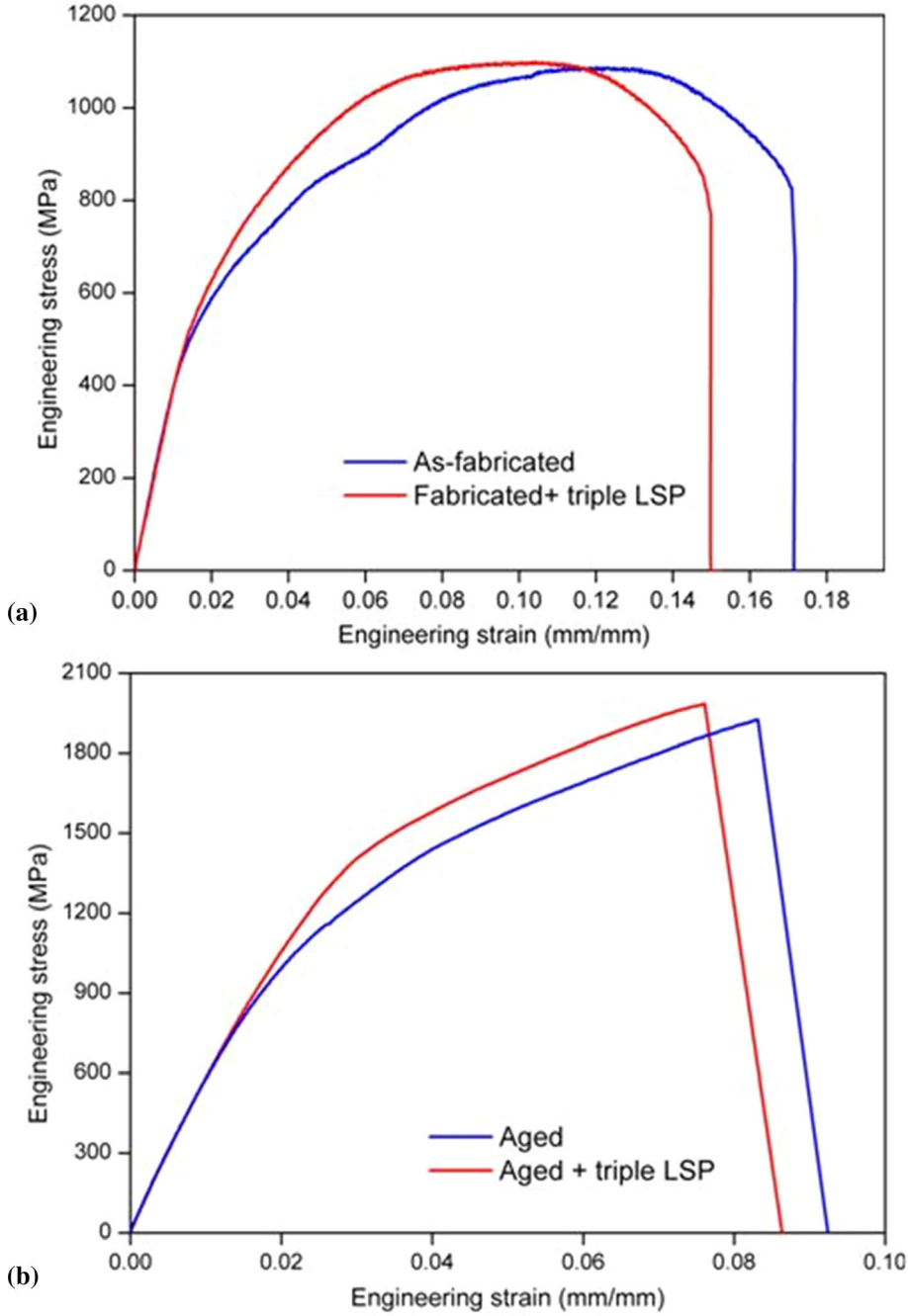

Fig. 13. Tensile curve of (a) F and (b) F+A samples before and after triple LSP

15.5% for triple LSP samples. Further, for F+A sample, a decrease in elongation from 9.2% to 8.4% for triple LSP sample is observed. The increase in YS for F and F+A DMLS Maraging steel shows that LSP facilitates to increase the ability of material for plastic deformation leading to an increase in the fatigue behavior. A summary of tensile properties obtained from the engineering stress-strain data of F and F+A samples before and after LSP is shown in Table 3.

4. Discussion

Development of Maraging grade steel using laser-based direct energy deposition techniques is touted as one of the promising areas in the industry (Ref 1, 2). However, the LAM based as built components cannot be directly used in service due to one of the inherent demerits that is high tensile residual stresses arising in the components due to high cooling rates (Ref 13). The presence of tensile residual stress in the LAM built components is the main cause of poor fatigue life and other mechanical properties (Ref 2).

In recent times, to minimize such undesired residual stresses present in the as built components, laser shock peening is used

Table 3. Tensile properties of F and F+A samples before and after triple LSP

Tensile properties	F	F + triple LSP	F+A	F+A + triple LSP
YS, MPa	753±10	850±14	1740±42	1910±43
UTS, MPa	1082±62	1120±48	1940±24	2040±34
El, %	17.5±1.0	15.6±0.8	9.1±0.7	8.5±0.4

as a post processing tool (Ref 28). In Additive Manufactured Ti and Al-based alloys, LSP treatment has been used successfully to improve the fatigue properties, tensile strength and corrosion resistance (Ref 12–15). In a similar manner, in the present study, multiple laser shock peening treatment of Maraging steel at the as-fabricated and aged conditions led to the induction of high compressive residual stress up to a significant depth which has been confirmed by residual stress measurement on the surface as well as along the depth (refer to Fig. 9 and 10). In addition, LSP treatment also led to an increase in the fraction of martensitic phase in both the as-fabricated and aged samples due to deformation induced martensitic transformation. The extent of increase in martensitic phase fraction in single peened samples with the as-fabricated condition is very high compared to the unpeened sample. This can be clearly witnessed from the first doublet XRD peak of Fig. 4. Further, with increase in LSP impacts to double and triple, the intensity of martensite phase increases marginally. This happens due to the saturation of deformation for higher laser impacts. In addition, if one looks at the XRD peaks of martensitic phase in aged samples (refer to Fig. 5), the increase in peak intensity due to LSP treatment is not very significant as compared to the as built samples. This could have arisen due to the fact that in the aged samples, the matrix become harder due to precipitation (hardness-570 HV), and applied shock wave pressure might be not that high to form enough martensite phase as compared to the as built samples (hardness 400 HV) (Ref 12).

In addition, from Fig. 6(a) and (b), it is clear that the peak broadening in single peened sample is not very significant; however, it increases for high angle peaks, which is generally expected. On the other hand, in the case of double and triple peened samples the broadening is significant but it is worth noting here that the broadening experienced by all the set of planes is not identical, as the increase of FWHM with diffraction angles is not monotonic. This kind of non-uniform broadening in bcc metals is already well reported during deformation and is attributed to the creation of stacking fault layers in certain planes due to the complex slip system operating in bcc metals (Ref 7). It may be further recalled that the fluctuation in W-H plot (refer to Fig. 7 and 8) is more dominant in double and triple peened samples in comparison to the single peened one, which is a signature of non-uniform broadening. Anisotropic deformation is more dominant in multiple peened samples and is attributed to the creation of stacking fault layer (Ref 28). Further, with an increase in laser impacts from single to triple, the crystallite size is found to decrease from 57 to 34 nm in the as-fabricated samples and from 76 to 41 nm in the aged samples. The decrease in crystallite size with increase in laser impacts arises due to severe plastic deformation at high strain rate during the peening process. It is well reported that grain refinement during plastic deformation at ultra-high strain rate is basically due to the generation of high-density dislocations and their annihilation as well as recombination during further deformation (Ref 7, 13). The decrease in grain size is further supported by an increase in hardness data post to multiple laser impacts (refer to Fig. 11 and 12). From these figures, it can be seen that for triple peening the extent of increase in hardness is more prominent in both the as-fabricated and aged sample when compared to single peened samples.

In a similar way, the effect of multiple laser peening on compressive residual stress can also be witnessed from Fig. 9 and 10. The increase in depth of compressive residual stress in the as-fabricated sample post to peening is higher than the aged sample. This actually depends on the attenuation of laser shock wave in the material and decided by the dynamic yield strength (Ref 28). In the case of multiple laser peening, the shock wave experiences lesser attenuation while passing through the work hardened surface layer generated by its preceding LSP treatment. As a result, it produces deeper compressively stressed surface layer (Ref 7, 13).

Further, it may be inferred from Fig. 10 that in the laser peened as-fabricated and aged samples, the CRS become zero beyond a certain depth. This happens due to the fact that beyond this depth the shock wave pressure in not enough to cause further deformation in the material. Thus, it is clear that with multiple peening the residual stress at the surface becomes homogeneous and also led to peening effect at larger depths in the material. Similar residual stress distribution has been observed in laser peened titanium and aluminum alloys, and it also found that beyond four LSP impacts the compressive residual surface stress get saturated at surface as well along depth (Ref 12-15). Further, as a result of the generation of high CRS in peened samples, the tensile properties such as yield strength and UTS are also increased. However, the Young's modulus is unchanged. The increase in tensile properties of LSP treated samples resulted due to the formation of sub-grain, mechanical twins and high-density dislocations (Ref 28). Due to the creation of sub-grain boundary and mechanical twins, the hardenability of material increases which in turn results in higher UTS and YS of LSP treated Maraging steel. Further, no change in Young's modulus is attributed to the fact that it is not a microstructure dependent property.

5. Conclusions

In the present study, effect of multiple laser shock peening on phase evolution, residual stress and mechanical properties of the as-fabricated and aged DMLS Maraging 300 steel is studied using various characterization techniques. From the above study, the following conclusions can be drawn:

I. X-ray-based analysis shows that LSP treatment led to an increase in phase fraction of the martensite phase in both

the as-fabricated and the aged samples due to the deformation induced martensitic transformation.

II. Broadening of XRD peaks confirm the nano sub-grain formation and creation of an inhomogeneous strain in the LSP treated samples. With an increase in LSP impacts, the sub-grain size is found to reduce for both the as-fabricated and aged samples.

III. Peening on DMLS fabricated Maraging 300 steel samples with single LSP impact at a laser power density of 3.9 GW cm^{-2} led to a significant increase in the compressive residual stress (of the order of −520 MPa (for the as-fabricated) and −550 MPa (for the aged) in comparison to the unpeened sample (-280 MPa)). However, with increasing number of laser impacts, it has marginally (–50 MPa) improved on the surface of both sample types. Multiple peening led to the presence of CRS to a depth of 675 μm in the as-fabricated sample and 340 μm in the aged samples.

IV. After triple peening, the hardness on the surface is found to be increased by 6.5% in the as-fabricated and by 13.2% in the aged samples. Further, along the depth the hardness is found to reduce and reached to a base value at different hardened layer depth for both the as-fabricated (250 μm) and the aged samples (220 μm). The hardened layer depth for single and double peened samples is found to be smaller than the triple peened one.

V. After triple LSP, the YS is increased by 12.8% for the as-fabricated sample and 9.7% for the aged samples when compared to the unpeened samples with reduced ductility. The change in UTS is found to be very small, and no change on Young's modulus is observed.

VI. This research facilitates to improve the mechanical properties and proves LSP to be an effective surface treatment method for DMLS Maraging steel.

Acknowledgments

Thanks are largely due to Dr. A.B. Nayak at Central Tool Room and Training Center, Bhubaneswar, India for extending the DMLS AM facilities. The support of Mr. D. C. Nagpure at LMPD, RRCAT Indore, India in measuring residual stresses is gratefully acknowledged. The lead author acknowledges the support of Ministry of Human Resource Development, Government of India for financial assistance as research fellowship. This research did not receive any specific grant from funding agencies in the public, commercial or not-for-profit sectors.

References

1. G. Casalino, S.L. Campanelli, N. Contuzzi and A.D. Ludovico, Experimental Investigation and Statistical Optimisation of the Selective Laser Melting Process of a Maraging Steel, *Opt. Laser Technol.*, 2015, **65**, p 151–158
2. J. Suryawanshi, K.G. Prashanth and U. Ramamurty, Tensile, Fracture, and Fatigue Crack Growth Properties of a 3D Printed Maraging Steel Through Selective Laser Melting, *J. Alloy Compd.*, 2017, **725**, p 355–364
3. D.D. Gu, W. Meiners, K. Wissenbach and R. Poprawe, Laser Additive Manufacturing of Metallic Components: Materials, Processes and Mechanisms, *Int. Mater. Rev.*, 2012, **57**, p 133–164
4. I. Gibson, D.W. Rosen and B. Stucker, *Additive Manufacturing Technologies: Rapid Prototyping to Direct Digital Manufacturing*, Springer, Boston, 2009, p 1–14
5. N. Kalentics, E. Boillat, P. Peyre, C. Gorny, C. Kenel, C. Leinenbach, J. Jhabvala and R.E. Logé, 3D Laser Shock Peening—A New Method for The 3D Control of Residual Stresses in Selective Laser Melting, *Mater. Design*, 2017, **130**, p 350–356
6. P. Ganesh, R. Sundar, H. Kumar, R. Kaul, K. Ranganathan, P. Hedaoo, G. Raghavendra, S.A. Kumar, P. Tiwari, D.C. Nagpure, K.S. Bindra, L.M. Kukreja and S.M. Oak, Studies on Fatigue Life Enhancement of Pre-Fatigued Spring Steel Specimens Using Laser Shock Peening, *Mater. Design*, 2014, **54**, p 734–741
7. A.K. Rai, R. Biswal, R.K. Gupta, S.K. Rai, R. Singh, P. Ganesh, R. Kaul and K.S. Bindra, Study on the Effect of Multiple Laser Shock Peening on Residual Stress and Microstructural Changes in Modified 9Cr-1Mo (P91) Steel, *Surf. Coat. Technol.*, 2019, **358**, p 125–135
8. J.Z. Lu, L. Zhang, A.X. Feng, Y.F. Jiang and G.G. Cheng, Effects of Laser Shock Processing on Mechanical Properties of Fe–Ni Alloy, *Mater. Design*, 2009, **30**, p 3673–3678
9. P. Ganesh, R. Sundar, H. Kumar, R. Kaul, K. Ranganathan, P. Hedaoo, P. Tiwari, L.M. Kukreja, S.M. Oak, S. Dasari and G. Raghavendra, Studies on Laser Peening of Spring Steel for Automotive Applications, *Opt. Lasers Eng.*, 2012, **50**, p 678–686
10. S. Keller, S. Chupakhin, P. Staron, E. Maawad, N. Kashaev and B. Klusemann, Experimental and Numerical Investigation of Residual Stresses in Laser Shock Peened AA2198, *J. Mater. Process. Technol.*, 2018, **255**, p 294–307
11. Y. Fan, Y. Wang, S. Yukelic and Y.L. Yao, Wave–Solid Interactions in Laser-Shock Induced Deformation Processes, *J Appl Phys.*, 2005, **98**, p 104904
12. J. Lu, H. Lu, X. Xu, J. Yao, J. Cai and K. Luo, High-Performance Integrated Additive Manufacturing With Laser Shock Peening—Induced Microstructural Evolution and Improvement in Mechanical Properties of Ti6al4v Alloy Components, *Int. J. Mach. Tools Manuf.*, 2020, **148**, p 103475
13. R. Sun, L. Li, Y. Zhu, W. Guo, P. Peng, B. Cong, J. Sun, Z. Che, B. Li, C. Guo and L. Liu, Microstructure, Residual Stress and Tensile Properties Control of Wire-Arc Additive Manufactured 2319 Aluminum Alloy With Laser Shock Peening, *J. Alloy Compd.*, 2018, **747**, p 255–265
14. S. Luo, W. He, K. Chen, X. Nie, L. Zhou and Y. Li, Regain the Fatigue Strength of Laser Additive Manufactured Ti Alloy Via Laser Shock Peening, *J. Alloy Compd.*, 2018, **750**, p 626–635
15. L. Petan, J.L. Ocana and J. Grum, Influence of Laser Shock Peening Pulse Density and Spot Size on the Surface Integrity of X2NiCoMo18-9-5 Maraging steel, *Surf. Coat. Technol.*, 2016, **307**, p 262–270
16. A. Salimianrizi, E. Foroozmehr, M. Badrossamay and H. Farrokhpour, Effect of Laser Shock Peening on Surface Properties and Residual Stress of Al6061-T6, *Opt. Lasers Eng.*, 2016, **77**, p 112–117
17. L. Chen, X. Ren, W. Zhou, Z. Tong, S. Adu-Gyamfi, Y. Ye and Y. Ren, Evolution of Microstructure and Grain Refinement Mechanism of Pure Nickel Induced by Laser Shock Peening, *Mat. Sci. Eng. A*, 2018, **728**, p 20–29
18. T. Bhardwaj and M. Shukla, Effect of Laser Scanning Strategies on Texture, Physical and Mechanical Properties of Laser Sintered Maraging Steel, *Mat. Sci. Eng. A*, 2018, **734**, p 102–109
19. C.S. Montross, T. Wei, L. Ye, G. Clark and Y.W. Mai, Laser shock Processing and its Effects on Microstructure and Properties of Metal Alloys: A Review, *Int. J. Fatigue*, 2002, **24**, p 1021–1036
20. S. Wei, G. Wang, L. Wang and Y. Rong, Characteristics of Microstructure and Stresses and their Effects on Interfacial Fracture Behavior for Laser-Deposited Maraging Steel, *Mater. Design*, 2018, **137**, p 56–67
21. J. Wang, Y. Lu, D. Zhou, L. Sun, L. Xie and J. Wang, Mechanical Properties and Microstructural Response of 2A14 Aluminum Alloy Subjected to Multiple Laser Shock Peening Impacts, *Vacuum*, 2019, **165**, p 193–198
22. N. Kalentics, E. Boillat, P. Peyre, S. Ciric-Kostic, N. Bogojevic and R.E. Logé, Tailoring Residual Stress Profile of Selective Laser Melted Parts by Laser Shock Peening, *Addit. manuf.*, 2017, **16**, p 90–97
23. W. Guo, R. Sun, B. Song, Y. Zhu, F. Li, Z. Che, B. Li, C. Guo, L. Liu and P. Peng, Laser Shock Peening of Laser Additive Manufactured Ti6Al4V Titanium Alloy, *Surf. Coat. Technol.*, 2018, **349**, p 503–510

24. N. Kalentics, K. Huang, M.O.V. de Seijas, A. Burn, V. Romano and R.E. Logé, Laser Shock Peening: A Promising Tool for Tailoring Metallic Microstructures in Selective Laser Melting, *J. Mater. Process. Technol.*, 2019, **266**, p 612–618
25. J. Li, J. Zhou, A. Feng, S. Huang, X. Meng, Y. Sun, Y. Huang and X. Tian, Influence of Multiple Laser Peening on Vibration Fatigue Properties of TC6 Titanium Alloy, *Opt. Laser Technol.*, 2019, **118**, p 183–191
26. K.Y. Luo, B. Liu, L.J. Wu, Z. Yan and J.Z. Lu, Tensile Properties, Residual Stress Distribution and Grain Arrangement as a Function of Sheet Thickness of Mg-Al-Mn Alloy Subjected to Two-Sided and Simultaneous LSP Impacts, *Appl. Surf. Sci.*, 2016, **369**, p 366–376
27. R.C. Picu, G. Vincze, F. Ozturk, J.J. Gracio, F. Barlat and A.M. Maniatty, Strain Rate Sensitivity of the Commercial Aluminium Alloy AA5182-O, *Mater. Sci. Eng. A.*, 2005, **390**, p 334–343
28. L. Hackel, J.R. Rankin, A. Rubenchik, W.E. King and M. Matthews, Laser Peening: A Tool for Additive Manufacturing Post-Processing, *Add. Manuf.*, 2018, **24**, p 67–75